OXFORD

SOT | Society of Toxicology
www.toxsci.oxfordjournals.org

TOXICOLOGICAL SCIENCES, 150(1), 2016, 40–53

doi: 10.1093/toxsci/kfv258
Advance Access Publication Date: November 25, 2015
Research Article

Proinflammatory Effects of Pyrogenic and Precipitated Amorphous Silica Nanoparticles in Innate Immunity Cells

Luisana Di Cristo,[*,†] Dania Movia,[†,‡] Massimiliano G. Bianchi,[*] Manfredi Allegri,[§] Bashir M. Mohamed,[†] Alan P. Bell,[¶] Caroline Moore,[†] Silvana Pinelli,[*] Kirsten Rasmussen,[||] Juan Riego-Sintes,[||] Adriele Prina-Mello,[†,‡] Ovidio Bussolati,[§,1] and Enrico Bergamaschi[*]

[*]Department of Clinical and Experimental Medicine, University of Parma, Parma, Italy; [†]School of Medicine and [‡]AMBER centre (CRANN Institute), Trinity College Dublin, Dublin, Ireland; [§]Department of Biomedical, Biotechnological and Translational Sciences, University of Parma, Parma, Italy; [¶]Advanced Microscopy Laboratory, Trinity College Dublin, Dublin, Ireland; [||]Joint Research Centre, Institute for Health and Consumer Protection, Ispra, Italy

[1]To whom correspondence should be addressed at Department of Biomedical, Biotechnological and Translational Sciences, University of Parma, Via Volturno 39, Parma 43125, Italy. Fax: +39 0521033742. E-mail: ovidio.bussolati@unipr.it

ABSTRACT

Amorphous silica nanoparticles (ASNP) can be synthetized via several processes, 2 of which are the thermal route (to yield pyrogenic silica) and the wet route from a solution containing silicate salts (to obtain precipitated, colloidal, mesoporous silica, or silica gel). Both methods of synthesis lead to ASNP that are applied as food additive (E551). Current food regulation does not require that production methods of additives are indicated on the product label, and, thus, the ASNP are listed without mentioning the production method. Recent results indicate, however, that pyrogenic ASNP are more cytotoxic than ASNP synthesized through the wet route. The present study was aimed at clarifying if 2 representative preparations of ASNP, NM-203 (pyrogenic) and NM-200 (precipitated), of comparable size, specific surface area, surface charge, and hydrodynamic radius in complete growth medium, had different effects on 2 murine macrophage cell lines (MH-S and RAW264.7 cells). Our results show that, when incubated in protein-rich fluids, NM-203 adsorbed on their surface more proteins than NM-200 and, once incubated with macrophages, elicited a greater oxidative stress, assessed from *Hmox1* induction and ROS production. Flow cytometry and helium ion microscopy indicated that pyrogenic NM-203 interacted with macrophages more strongly than the precipitated NM-200 and triggered a more evident inflammatory response, evaluated with *Nos2* induction, NO production and the secretion of TNF-α, IL-6 and IL-1β. Moreover, both ASNP synergized macrophage activation by bacterial lipopolysaccharide (LPS), with a higher effect observed for NM-203. In conclusion, the results presented here demonstrate that, compared to precipitated, pyrogenic ASNP exhibit enhanced interaction with serum proteins and cell membrane, and cause a larger oxidative stress and stronger proinflammatory effects in macrophages. Therefore, these 2 nanomaterials should not be considered biologically equivalent.

Key words: amorphous silica nanoparticles; food additive; inflammation; macrophages; oxidative stress; protein corona

Amorphous silica nanoparticles (ASNP) are integrated in a wide variety of commercial products for human use, such as pharmaceutical products, paints, cosmetics, and food. ASNP can be synthetized through 2 main methods, the high-temperature thermal route, to yield *pyrogenic silica,* or low-temperature wet routes to form *precipitated*, *colloidal*, *mesoporous* silica, or *silica gel* (Napierska *et al.*, 2010). ASNP are produced in tonnage quantities and are, therefore, among the most abundant synthetic nanoparticles currently available on the market. In the last decades, ASNP produced by either thermal or wet methods are used in food, eg as an anticaking agent for food products in powder form, to remove yeast and protein from beer, as an antifoaming agent for wine and as a viscosity control for pastes (eg, ketchup) and other food. ASNP are indicated on the label of the food as the food additive E551 without specification of the production process of the nanomaterial.

The potential toxicity of ASNP has been extensively investigated in several studies (please refer to (Napierska *et al.*, 2010) for a comprehensive review), and experimental evidence of a dose-dependent oxidative stress, cytotoxicity, and inflammatory effects has been reported (Athinarayanan *et al.*, 2014; Lin *et al.*, 2006; Morishige *et al.*, 2010a; Park and Park, 2009). Given that the production process strongly influences surface reactivity (Napierska *et al.*, 2010), several studies take into account its possible implications for the toxicological behavior of ASNP. For instance, Zhang *et al.* (2012) found that the lung toxicity of pyrogenic ASNP was comparable to or even exceeding that of crystalline silica nanoparticles, known since many years to be highly toxic (Fubini and Hubbard, 2003). Moreover, relatively high doses of pyrogenic ASNP resulted in rat liver fibrosis after 84 days of exposure (van der Zande *et al.*, 2014). However, also ASNP produced with wet methods have been found to be endowed with some toxicity (Kaewamatawong *et al.*, 2005; Morishige *et al.*, 2010b; Nishimori *et al.*, 2009). As far as precipitated ASNP are concerned, they have been found to produce only transient and reversible neutrophilic lung inflammatory responses at 24 h (Sayes *et al.*, 2007). In addition, precipitated ASNP seem nearly inert when assayed for hemolytic activity (Pavan *et al.*, 2013) and failed to induce significant increases in the frequency of micronucleated binucleate cells (MNBCs) in human lymphocyte populations (Tavares *et al.*, 2014).

However, only a few studies directly compare the toxicity of pyrogenic and precipitated ASNP. An inhalation toxicity study in Wistar rats (Arts *et al.*, 2007) demonstrated that pyrogenic silica induced a more pronounced increase in the expression of lung inflammation markers and, although equally cleared from the tissue, produced more severe histopathological changes than the precipitated form. The structural determinants for this different biological reactivity have been recently investigated using an *in vitro* model (Guichard *et al.*, 2015). The results presented in that study suggested that the cytotoxicity and genotoxic properties of ASNP are related more to the primary particles size or to the agglomeration than to the production process. On the contrary, other studies attributed the increased cytotoxicity and proinflammatory activating effects of pyrogenic ASNP to their higher surface reactivity (Gazzano *et al.*, 2012; Sandberg *et al.*, 2012) or fused chainlike morphology (Zhang *et al.*, 2012). Since pyrogenic and precipitated ASNP of different size and specific surface area were used in these contributions, the question is open if these physicochemical characteristics contributed to the dissimilar toxicological behavior of the ASNP tested. For instance, due to these different physicochemical characteristics, the expression of the biological activities of pyrogenic or precipitated ASNP per mass unit or per surface unit led either to consistent (Gazzano *et al.*, 2012) or contrasting conclusions on their relative toxicity ranking (Sandberg *et al.*, 2012).

To address this issue, here we compare the ability of 2 representative manufactured nanomaterials of comparable size and specific surface area to exert toxic effects and to induce cell activation in 2 murine macrophage cell lines.

MATERIALS AND METHODS

Reagents. Fetal bovine serum (FBS) and culture media were purchased from Euro-Clone SpA, Pero, Milan, Italy. CM-H_2DCF-DA was purchased from Molecular Probes, Invitrogen, (Milan, Italy). Sigma-Aldrich (Milan, Italy) was the source of LPS (from *E. coli*, O55:B5 serotype) and of all the other chemicals, whenever not specified otherwise.

Amorphous silica nanoparticles (ASNP). ASNP samples (NM-200 and NM-203) were obtained from the JRC Nanomaterials Repository hosting representative industrial nanomaterials (Ispra, Varese, Italy). These materials are classified as representative test materials (RTM) and include a (random) sample from 1 industrial production batch. They are used within the scope of the EU FP7 project "Managing risks of nanomaterials (MARINA)".

NM-200 are precipitated silica produced by wet route, in which a solution of alkali metal silicate is acidified to produce a gelatinous precipitate that is washed and then dehydrated to produce colourless microporous silica particles (Rasmussen *et al.*, 2013). NM-203 are pyrogenic silica produced via the thermal route, that is burning $SiCl_4$ in an oxygen-rich hydrocarbon flame to produce a fume of SiO_2 (Rasmussen *et al.*, 2013).

Transmission electron microscopy (TEM). ASNP were dispersed into 0.05 wt% BSA in water, at the concentration of 2.56 mg/ml. The TEM specimens of suspended ASNP were prepared on 300-mesh Cu lacey carbon grids by drop-casting and were visualized under a Jeol 2100 Transmission Electron Microscope (Jeol Ltd., Tokyo, Japan) operating at 200 kV with a Lanthanum Hexaborise emission source.

Nanoparticle tracking analysis. The average hydrodynamic radius of NM-200 and NM-203 in complex dispersion media was characterised using nanoparticle tracking analysis (NTA) developed by Malvern Instruments Limited (Wiltshire, UK). This technique utilises the properties of light scattering and Brownian motion to obtain particle size distributions of samples in liquid suspension (Hole *et al.*, 2013). A NS500 instrument, equipped with a 405 nm laser in conjunction with software version NTA 3.1, was used for the purpose of this study. NM-200 and NM-203 were dispersed in 0.05% BSA-water and sonicated for 15 min with a Branson 5510 sonication bath prior to incubation in the various media, ie, water, nonsupplemented RPMI1640 medium (Gibco, Life Technologies, cat no. 61870) and RPMI medium supplemented with 10% FBS at 3 different concentrations (16, 32, and 64 μg/ml). Hydrodynamic radius was measured after incubation at 37°C for 0 and 24 h. A nanoparticles concentration that records a minimum of 200 tracks per video was undertaken to obtain statistical significance. Five by 60 s videos were recorded for each sample. Results are reported as average mode ± standard deviation.

Protein adsorption to ASNP. ASNP were incubated for 1 h at 37°C in RPMI culture medium with 10% FBS. At the end of the incubation, the suspension was centrifuged for 15 min at 13000 *g*, and the pellets were washed 3 times in 18 mΩ water. Proteins

adsorbed to the ASNP were then quantified with a modified micro Lowry protein assay (Farinha *et al.*, 2004) or separated on a 12% (w/v) SDS-PAGE gel. For PAGE, pellets were suspended in Laemmli buffer 1× (250 mM Tris–HCl, pH 6.8, 8% SDS, 40% glycerol, and 0.4M DTT), warmed at 95°C for 10 min, and aliquots of 25 µl were loaded on gel. The gel was then washed 3 times in 18 mΩ water and stained through silver staining (Cosmo Bio Co., Ltd., Tokyo, Japan, Cat. No. 423413) according to manufacturer's instructions. The intensity of the protein bands was determined with a Personal Densitometer SI Molecular Dynamics (GE Healthcare Europe GmbH, Milano, Italy) after further staining with Bio-Safe™ Coomassie G-250 Stain (Cat. 161-0786, Bio-Rad Laboratories S.r.l., Milan, Italy) to increase band intensity.

Cell culture. Murine alveolar macrophages (MH-S), a gift of Prof. Dario Ghigo, University of Torino (Italy), were originally provided by the Cell Bank of the Istituto Zooprofilattico Sperimentale della Lombardia ed Emilia-Romagna (Brescia, Italy). RAW264.7 murine peritoneal macrophages were obtained from the Cell Bank of the Istituto Zooprofilattico Sperimentale della Lombardia ed Emilia-Romagna (Brescia, Italy). Cells were routinely cultured in a humidified atmosphere of 5% CO_2 in air in Falcon 10-cm diameter dishes (BD, Bioscience, USA) or in T75 cell culture flasks (Nunc, Fisher Scientific, Ireland) in RPMI1640 medium supplemented with 10% FBS, streptomycin (100 µg/ml)–penicillin (100 U/ml), L-glutamine (2 mM), and (for MH-S cells only) β-mercaptoethanol (0.05 mM). For experiments, cells were seeded in complete growth medium in Falcon 24-well plates (BD Bioscience, San Jose, California, USA) or Millicell EZ 4-well glass slides (Millipore, Ireland) at a density of 20×10^4 cells/well.

Incubation with ASNP and dosimetry. Before the experiments, ASNP were heated at 230°C for 4 h to eliminate possible contamination from lipopolysaccharide (LPS). After cooling at room temperature, nanomaterials were dispersed in a stock solution at a concentration of 2.5 mg/ml by pre-wetting powder in 0.5% ethanol (96% purity) followed by dispersion in 0.05 wt% bovine serum albumin (BSA, A9418, Sigma Aldrich) in water and 16 min of bath sonication (from Nanogenotox protocol, with modifications). The ASNP suspensions thus obtained were diluted in complete growth medium to reach the desired dose.

Taking into account the volume/surface ratio of the various culture systems adopted and the use of subconfluent (for cytotoxicity experiments) or confluent monolayers (for other studies), we have expressed the ASNP nominal doses as µg of materials per cm^2 of monolayer. The volume/culture surface ratio has been kept constant in all the experiments. The dosimetry of nanomaterials, expressed as µg/ml or m^2/ml, is summarized in Table 1.

High content screening and analysis (HCSA)–ASNP cytotoxicity. MH-S and RAW264.7 cells were exposed to increasing doses (2.5, 5, 10, 20, 40, 80 µg/cm^2) of ASNP for 24, 48, and 72 h. Data are reported as average standard deviation ($n_{replicates} = 3$; $n_{tests} = 3$). Positive (cells exposed to cisplatin) and negative (untreated cells) controls were also included into each experiment in order to quantify the extent of toxicity response induced by each particle type. After, respectively, 24, 48, and 72 h of incubation, cells were washed in phosphate-buffered saline solution (PBS) at pH 7.4 and fixed in 3% paraformaldehyde (PFA), as described previously (Mohamed *et al.*, 2011; Movia *et al.*, 2011; Movia *et al.*, 2010; Prina-Mello *et al.*, 2013; Williams *et al.*, 2008). Multiparametric analysis of the ASNP cytotoxicity response using HCSA was performed using the Cellomics® HCS reagents Cytotoxicity1 kit and Apoptosis1 kit (Thermo Fisher Scientific, Ireland) according to manufacturer's instructions. The kits allow detecting and quantifying changes in (1) cell count, lysosomal mass/pH, cell membrane permeability (as parameters recorded with the Cytotoxicity1 kit) and, (2) mitochondrial activity, cytoskeletal actin reorganisation, nuclear intensity, and nuclear size (as parameters recorded with the Apoptosis1 kit), which are phenomena associated to a toxicological response. Plates were analysed by IN Cell Analyzer 1000 automated microscope (GE Healthcare, Buckinghamshire, UK). Cytotoxicity and apoptosis responses were quantified using the analysis module of the IN Cell Investigator software (GE Healthcare). The module allows simultaneous quantification of subcellular inclusions that are marked by different fluorescent probes and measures fluorescence intensity associated with predefined nuclear and cytoplasmic compartments, as previously described (Prina-Mello *et al.*, 2014).

Table 1. Dosimetry of ASNP[a]

Doses (µg/cm^2)	Doses (µg/ml)	Doses (m^2/ml)	
		NM-200	NM-203
5	10	0.00189	0.00204
10	20	0.00378	0.00407

[a]Conversion of the doses used (5 or 10 µg/cm^2). The m^2/ml doses are calculated using the values of specific surface area of ASNP shown in Table 3.

Cellular internalization of ASNP. RAW264.7 cells were plated in 4-well Millicell™ EZ Slide (Merck SpA, Vimodrone, Milan, Italy) at a concentration of 20×10^4 cells/well. Cells were incubated for 24 h at 37°C (5% CO_2) to allow cell attachment to the glass substrate. For internalization, cells were incubated with ASNP at a concentration of 5 µg/cm^2. After 2 h, cells were transferred for 20 min into serum-free medium supplemented with CellTracker™ Red CMPTX (8 µM, Molecular Probes, Invitrogen) to label the cytoplasm; in the last 10 min 1,5-bis[2-(di-methylamino)ethyl]amino-4, 8-dihydroxyanthracene-9,10-dione (DRAQ5®, 20 µM, Alexis Biochemicals, San Diego, California, USA) was also added to the incubation medium to counterstain the nucleus. At the end of the incubation, cell monolayers were rinsed in PBS and fixed with 3.7% PFA at room temperature for 15 min. Specimens were then mounted on glass slides with fluorescence mounting medium (Dako Italia SpA, Milan, Italy) and imaged by confocal microscopy. Confocal analysis was carried out with a LSM 510 Meta scan head integrated with an inverted microscope (Carl Zeiss, Jena, Germany). Samples were observed through a 40× (1.4 NA) oil objective. Image acquisition was carried out in multitrack mode, ie, through consecutive and independent optical pathways. Excitation at 488 nm and reflectance were used to visualize ASNP (shown in green as pseudo-colour); excitation at 543 nm and emission recorded through a 580–630 nm band pass barrier filter were used to visualize the cytoplasm (red, pseudo-colour); excitation at 633 nm and emission through a 670 nm long pass filter were recorded to visualize the nucleus (blue, pseudo-colour).

Cytofluorimetric assay of ASNP uptake. The light scattered at a 90° angle to the axis of the laser beam is measured as side scatter (SSC) and is related to intracellular density, a parameter associated with ASNP uptake (Zhao and Ibuki 2015). For these experiments, RAW264.7 cells were seeded in 6-well plates at the density of 1×10^6 cells/well. After 30 min or 2 h of incubation with NM-200 or NM-203 (5 µg/cm^2), cells were washed with PBS,

Table 2. Primers and Temperatures of Annealing Adopted for RT-PCR Experiments

Gene	Protein	Forward Primer	Reverse Primer	T (°C)	Amplicon Size (bp)
Inducible nitric oxide synthetase (*Nos2*)	Inducible nitric oxide synthetase (Nos2)	5′-GTT CTC AGC CCA ACA ATA CAA GA-3′	5′-GTG GAC GGG TCG ATG TCA C-3′	57	127
Hemeoxygenase 1 (*Hmox1*)	Hemeoxygenase 1 (HO-1)	5′-AGG TAC ACA TCC AAG CCG AGA-3′	5′-CAT CAC CAG CTT AAA GCC TTC T-3′	57	86
Glyceraldehyde 3-phosphate dehydrogenase (*Gapdh*)	Glyceraldehyde 3-phosphate dehydrogenase (Gapdh)	5′-TGT TCC TAC CCC CAA TGT GT-3′	5′-GGT CCT CAG TGT AGC CCA AG-3′	57	137
Tumor necrosis factor (*Tnf*)	Tumor necrosis factor-alpha (TNF-α)	5′-CCC TCA CAC TCA GAT CAT CTT C-3′	5′-GCT ACG ACG TGG GCT ACA G-3′	55	61

detached with a cell scraper and analysed by a FC500^{TM} flow cytometer (Beckman Coulter, Brea, California, USA), as described previously (Alinovi *et al.*, 2015) The cytograms and the histogram were obtained using FlowJo software (Ashland, Oregon, USA).

He-ion microscopy (HIM). Cells were fixed at room temperature in 2.5% glutaraldehyde in 0.1 M Sørensen's phosphate buffer (pH 7.3) and rinsed with Sørensen's phosphate buffer. Samples were dehydrated in increasing concentrations of EtOH (from 70% up to 100%). The final wash was carried out in pure EtOH for 20 min. The samples were air dried and imaged by a Zeiss Orion Plus He-ion microscope (Carl Zeiss, Oberkochen, Germany) using an accelerating voltage of 30 kV. Samples were transferred into the chamber, which had undergone plasma clean overnight prior to loading samples, using a load lock. The working distance was 8 mm and a 10-μm beam limiting aperture was used. The probe current was between 0.5 and 1.5 pA. Images were acquired by collecting the secondary electrons emitted by the interaction between the He-ion beam and the specimen with an Everhart-Thornley detector (part of the He-ion microscope system). The image signal was acquired in a 32 - or 64-line integration to each contributing line of the image.

Gene expression analysis. The expression of *Nos2*, *Hmox1*, and *Tnf* was assessed with real Time PCR. 1 μg of total RNA, isolated with GenElute Mammalian Total RNA Miniprep Kit (Sigma–Aldrich) was reverse transcribed. For real-time qPCR, cDNA was amplified with Go Taq PCR Master Mix (Promega, Italia, Milan, Italy), along with the forward and reverse primers indicated in Table 2 (5 pmol each). The expression of the gene of interest under each experimental condition was normalized to that of *Gapdh* and shown relative to its expression level in control, untreated cells.

Cell lysis and Western blotting. Cells were lysed in a buffer containing 20 mM Tris–HCl, pH 7.5, 150 mM NaCl, 1 mM EDTA, 1 mM EGTA, 1% Triton, 2.5 mM sodium pyrophosphate, 1 mM β-glycerophosphate, 1 mM Na_3VO_4, 1 mM NaF, 2 mM imidazole and a cocktail of protease inhibitors (Complete, Mini, EDTA-free, Roche, Milan, Italy). Lysates were sonicated for 15 s and centrifuged at 12 000 *g* for 20 min at 4°C. After quantification with the Bio-Rad protein assay, aliquots of 40 μg of proteins were mixed with Laemmli buffer 4× (250 mM Tris–HCl, pH 6.8, 8% SDS, 40% glycerol, and 0.4 M DTT), warmed at 95°C for 10 min and loaded on a 8% gel for SDS-PAGE. After electrophoresis, proteins were transferred to PVDF membranes (Immobilon-P, Millipore, Millipore Corporation, Massachusetts, USA). Non-specific binding sites were blocked with an incubation of 1 h at room temperature in 5% BSA in TBS-Tween. The blots were then exposed at 4°C overnight to anti-Nos2 (rabbit polyclonal, 1:400, Santa Cruz Biotechnology) or antiactin (rabbit polyclonal, 1:30 000, Cell Signaling Technology diluted in the same solution). After washing, the blots were exposed for 1 h at room temperature to HRP-conjugated antirabbit antibody (Cell Signaling Technology), diluted 1:20 000 in blocking solution. Immunoreactivity was visualized with Immobilon Western Chemiluminescent HRP Substrate (Millipore, Milan, Italy).

Determination of NO production. Nitrite concentration in the culture media, as an indicator of NO production, was determined through a fluorometric approach, as previously described (Sala *et al.*, 2002). The method is based on the production of the fluorescent molecule 1H-naphthotriazole from 2,3-diaminonaphthalene (DAN) in acid environment. For nitrite determination, 100 μl of medium were put in wells of a black 96-well plate with a clear bottom (Corning, Cambridge, Massachusetts, USA). DAN (20 μl of a solution of 0.025 mg/ml in 0.31 M HCl) was then added and, after 10 min at room temperature, the reaction was stopped with 20 μl of 0.7 N NaOH. Standards were performed in the same medium from a solution of 1 mM sodium nitrite. Fluorescence was determined with an EnSpire plate reader (Perkin Elmer). Nitrite production was expressed in nmoles per ml of extracellular medium (μM).

Cytokine secretion. After the selected incubation periods in presence of ASNP, the presence of tumor necrosis factor-alpha (TNF-α), Interleukin-6 (IL-6), and IL-1β in the culture media of the MH-S and RAW264.7 was determined with ELISA RayBio® kits (Ray Biotech, Norcross, Georgia, USA). 100 μl of medium were transferred into 96-well plates functionalized with anti-cytokine antibodies and incubated overnight at 4°C. Then, 100 μl of biotinylated antiIgG-antibody were added in each well and, after 1 h of incubation at RT, 100 μl of streptavidin solution were added. After 45 min, samples were incubated with 100 μl of the TMB One Step Reagent, contained in the kit solution; after 30 min, reaction was stopped and absorbance was immediately read at 450 nm with a plate reader. Standards were performed in the assay buffer from a solution of 50 ng/ml of the recombinant cytokine, as per manufacturer's protocol.

Intracellular reactive oxygen species production. The production of ROS was measured using 5-(and-6)-chloromethyl-2′,7′ dichlorodihydrofluorescein diacetate, acetyl ester (CM-H_2DCF-DA, Cat. No. C6827, Molecular Probes, Invitrogen). After the experimental treatments, cells were incubated with the probe (5 μM) for 2 h at 37°C. Cells were then washed twice with PBS and the fluorescence was determined (485 nm λ_{ex} and 520 nm λ_{em}) with a multiplate reader. Hydrogen peroxide (6 mM, 1 h before adding the probe) was used as a positive control. Cell fluorescence was

visualized using a fluorescence microscope (Nikon, Tokyo, Japan).

Statistics and data presentation. Statistic evaluation of effects has been performed with 2-tail t test for unpaired data to compare positive (LPS in Figs. 4 and 5 and 6 E-F; H_2O_2 in Figs. 6A and B) and negative controls. One-way ANOVA with Tukey test has been used in all the other cases. Statistical evaluations have been performed using GraphPad Prism™ software version 4.00 (GraphPad Software Inc., San Diego, California, USA). Differences have been considered significant for values of $P < .05$. In order to screen and normalise the results of High Content Screening, KNIME in combination with a screening module HiTS (http://code.google.com/p/hits, 0.3.0) were implemented as previously described (Kozak *et al.*, 2010; Williams *et al.*, 2008). All measured parameters were normalized using the percent of the positive controls. Z score was used for scoring the normalized values. These scores were summarized using the mean function as follows Z score= (x-mean)/StDev, as from previous work (Birmingham *et al.*, 2009; Movia *et al.*, 2011; Movia *et al.*, 2010; Prina-Mello *et al.*, 2013; Williams *et al.*, 2008). Heatmap graphical illustration in a colorimetric gradient table format was adopted as the most suitable schematic representation to report on any statistical significance and variation from normalized controls based on their Z score value. Heatmap tables illustrate the range of variation of each quantified parameter from the minimum (green) through the mean (yellow) to the maximum (red) accordingly to the parameter under analysis.

RESULTS

Physicochemical Properties of ASNP

A detailed physicochemical characterization of the ASNP, provided in the report on the synthetic amorphous silicon dioxide nanomaterials of the JRC Repository (Rasmussen *et al.*, 2013), is summarized in Table 3.

The TEM images of NM-200 and NM-203 (Supplementary Fig. 1) indicated that both nanomaterials mainly consist of small aggregates of some elementary particles that tend to clump in larger agglomerates, while primary particles are rarely detected.

Table 4 reports the average hydrodynamic radius of each sample, at the maximal dose used in the biological experiments, in water, nonsupplemented medium and protein-supplemented medium, as recorded by NTA. A high standard deviation in the measurements of NM-200 and NM-203 samples dispersed in water and nonsupplemented culture medium was associated with a broad range in distribution of nanoparticles sizes and with agglomeration phenomena. ASNP dispersed in medium supplemented with 10% FBS showed a more mono-dispersed population. NM-203 showed a decreasing trend in hydrodynamic radius after 24 h incubation, indicating the breakdown of particle agglomerates. Interestingly, minor changes in the hydrodynamic radius of the 2 samples dispersed in supplemented medium were recorded over time, suggesting the stabilisation of the nanoparticle dispersion or formation of protein corona by FBS. Under conditions resembling those adopted for the biological experiments (ie, t = 24 h, RPMI supplemented with FBS) the hydrodynamic radius of NM-200 and NM-203 was comparable.

Binding of Serum Proteins to ASNP

In order to evaluate the binding of serum proteins with ASNP, NM-200, and NM-203 were incubated with culture medium supplemented with 10% FBS. Proteins adsorbed to ASNP were then quantified with a colorimetric method or detected with silver staining after polyacrylamide gel electrophoresis (Fig. 1). Quantification of adsorbed proteins (Fig. 1A) evidenced that ASNP bound serum proteins in a dose-dependent trend, with significantly higher amounts for NM-203 than for NM-200. The increased adsorption capability of NM-203 was confirmed with silver staining (Fig. 1B and C), for either FBS or pure BSA. The adsorbed protein pattern was different for the 2 ASNP types, with a few bands clearly more abundant in NM-200 than in NM-203 eluate.

Interaction of ASPN with Macrophages

MH-S and RAW264.7 cells were imaged by He-ion microscopy (HIM) after 24 h incubation with NM-200 and NM-203 (Fig. 2). Untreated cells (negative control) cultured for 24 h were also imaged for comparison (Fig. 2A and B, 2G and H). Many ASNP agglomerates could be found in close proximity of the exposed cells and, in some cases, cells surface was partially or completely

Table 4. Hydrodynamic Radius of NM-200 and NM-203 (at 64 μg/ml) as Determined by NTA

Water	Mode t:0 h	Mode t:24 h
NM-200	206.8 ± 25.1 nm	274.5 ± 87.2 nm
NM-203	349.5 ± 43.9 nm	170.6 ± 36.7 nm
RPMI medium		
NM-200	355.1 ± 96.2 nm	323.0 ± 97.3 nm
NM-203	304.3 ± 30.7 nm	262.3 ± 25.0 nm
RPMI medium + 10% FBS		
NM-200	129.1 ± 6.7 nm	137.3 ± 11.5 nm
NM-203	173.5 ± 14.0 nm	138.3 ± 16.4 nm

Table 3. Physicochemical Properties of the ASNP Tested[a]

Nanomaterial	Indicative Content of SiO_2 (%wt)[b]	Crystallinity	Primary Particle Size (nm)	Specific Surface Area (m^2/g)	Zeta Potential (Surface Charge)	Redox Potential
NM-200	96 (EDS)	amorphous	14 ± 7 (TEM)	189.16 (BET)	−47.5 (mV) (in milliQ water, at pH 7)	Inactive or reductive (Oxo Dish fluorescence, sensor plate for O_2 detection)
NM-203	99 (EDS)	amorphous	13 ± 6 (TEM)	203.92 (BET)	−46.1 (mV) (in milliQ water at pH 6.6)	Oxidative Reactivity (Oxo Dish fluorescence, sensor plate for O_2 detection)

[a]Data are taken from (Rasmussen *et al.*, 2013)
[b]The content of Si is 44.77 and 46.32 (%wt) for NM-200 and NM-203, respectively.

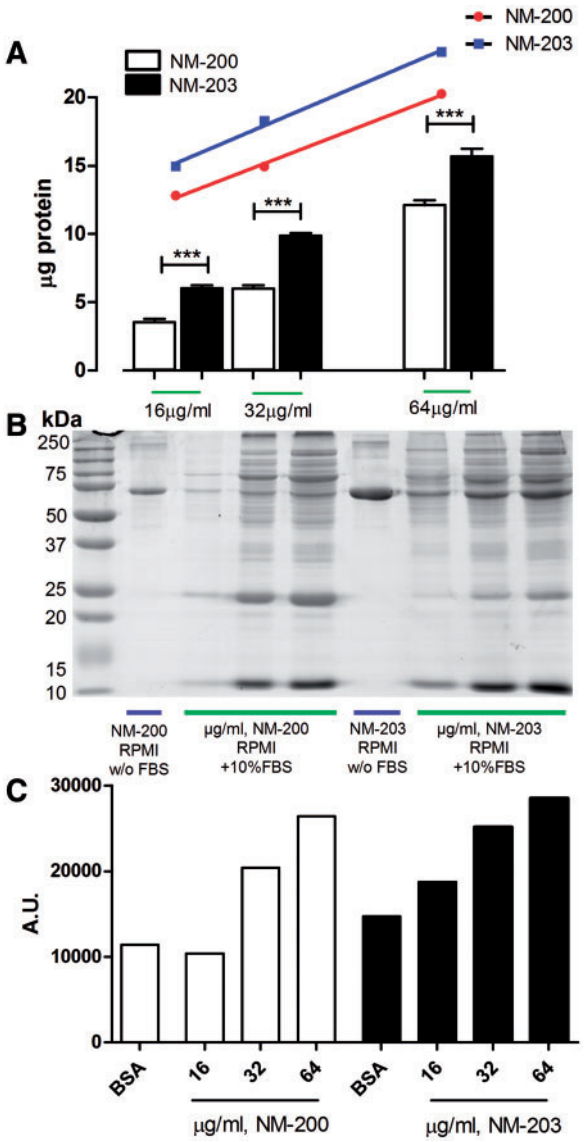

FIG. 1. Protein adsorption to ASNP. Nanoparticles, dispersed in 0.05 wt% BSA, were incubated at the concentration of 16-32-64 µg/ml for 1 h in culture medium with or without 10% FBS. At the end of the incubation, the suspensions were centrifuged, and adsorbed proteins quantified (A) or separated and stained (B and C), as described in Methods. C, shows the densitometric quantification of the lanes after silver staining. For (A), data are means ± SD of 3 independent determinations. $^{**}P < .01$ and $^{***}P < .001$. The lines shown in (A) are linear regression best fits. For NM-200: $y = 0.180\ x + 0.5$ ($r^2 = 0.9930$); for NM-203: $y = 0.198\ x + 3.11$ ($r^2 = 0.9894$). Slopes are statistically different ($P < .001$). For (B) and (C) a representative experiment, performed twice with comparable results, is shown. Abbreviations: ASNP, amorphous silica nanoparticles; BSA, bovine serum albumin; NM, nanomaterials.

covered by an ASNP layer. In particular, NM-203 (see the representative fields shown in Fig. 2E and F and 2M and N) formed agglomerates onto the cell surface more readily than NM-200 (Fig. 2C and D and 2I–L). Moreover, MH-S cells interacted with NM-200 agglomerates more closely than RAW264.7 cells.

Cell Internalization of ASNP

The internalization of ASNP was assessed in RAW264.7 cells after 2 h of incubation with confocal microscopy and cytofluorimetry. Images evidenced that both ASNP (imaged in reflectance mode) were effectively internalized into the macrophages (Supplementary Fig. 2). In addition, the cytogram distribution, recorded by cytofluorimetry, and the corresponding histograms (Fig. 3), showed an increase in SSC intensity after treatment with both ASNP for 30 min, thus suggesting that ASNP were rapidly taken up by the macrophages. However, the mean SSC ratio was higher for NM-203 than for NM-200 at both 30 min (17%) and 2 h (56%) of treatment, indicating a more efficient uptake of the pyrogenic ASNP.

Cytotoxicity of ASNP on Murine Macrophages

Recent data from our and other laboratories, obtained with several independent methods on a wide range of NM-200 and NM-203 doses at various incubation times (Farcal *et al.*, 2015), indicated that NM-203 cause a larger decrease in cell viability than NM-200 in both MH-S and RAW264.7 cell models.

Changes in cell count recorded and quantified by HCSA confirmed that NM-203 were more cytotoxic than NM-200 (Supplementary Figs. 3–6). Increased apoptotic response was also higher for NM-203 than NM-200-treated cells. Several other parameters also changed with different patterns suggesting that the interaction of the 2 nanomaterials with macrophages triggered various cytotoxicity and apoptotic pathways, as reported in the supplemental information section.

Macrophage Activation by Pyrogenic and Precipitated ASNP

Figure 4A reports *Nos2* mRNA expression after 24 h incubation of MH-S macrophages to non-cytotoxic doses (5 or 10 µg/cm^2) of NM-200 or NM-203. *Nos2* was significantly induced by incubation with NM-200 (at 10 µg/cm^2) or NM-203 (at both 5 and 10 µg/cm^2). This effect was confirmed at protein level (Fig. 4C) and corresponded to a clear cut increase in NO production (Fig. 4E). However, in RAW264.7 cells *Nos2* messenger was not significantly induced compared with control under the same experimental conditions (Fig. 4B), although, only in cells treated with NM-203, Nos2 protein appeared barely detectable and, consistently, increased accumulation of nitrites in the medium was observed (Fig. 4D–F).

Recently, a synergistic effect on macrophage activation has been described for TiO_2 NP and LPS (Bianchi *et al.*, 2015). To assess if also ASNP synergize LPS effects on macrophages, RAW264.7 cells were simultaneously treated with LPS and either ASNP (Fig. 4G). The combined treatment caused a further significant stimulation of NO production, compared with that observed after incubation with LPS alone. The enhancing effect was much higher for NM203-treated (+52%) compared to NM200-treated cells (+18%).

Secretion of Proinflammatory Cytokines in MH-S and RAW264.7 Cells Exposed to ASNP

The secretion of the proinflammatory cytokines TNF-α, IL-6, and IL-1β was quantified in the culture medium after the treatment of MH-S and RAW264.7 cells with NM-200 and NM-203 at 5 or 10 µg/cm^2 (Fig. 5). Under control conditions, the levels of the 3 cytokines in the culture medium were very low or below threshold. However, both cell lines produced a significant increase of medium TNF-α (assessed at 6 h of treatment), IL-6 (at 12 h), and IL-1β (after 48 h of treatment), although MH-S (Fig. 5A, C and E) cells consistently secreted more cytokines than RAW264.7 cells (Fig. 5B, D and F). At the higher dose used (10 µg/cm^2), and with both cell models, pyrogenic ASNP elicited a higher secretion of the 3 cytokines than precipitated ASNP.

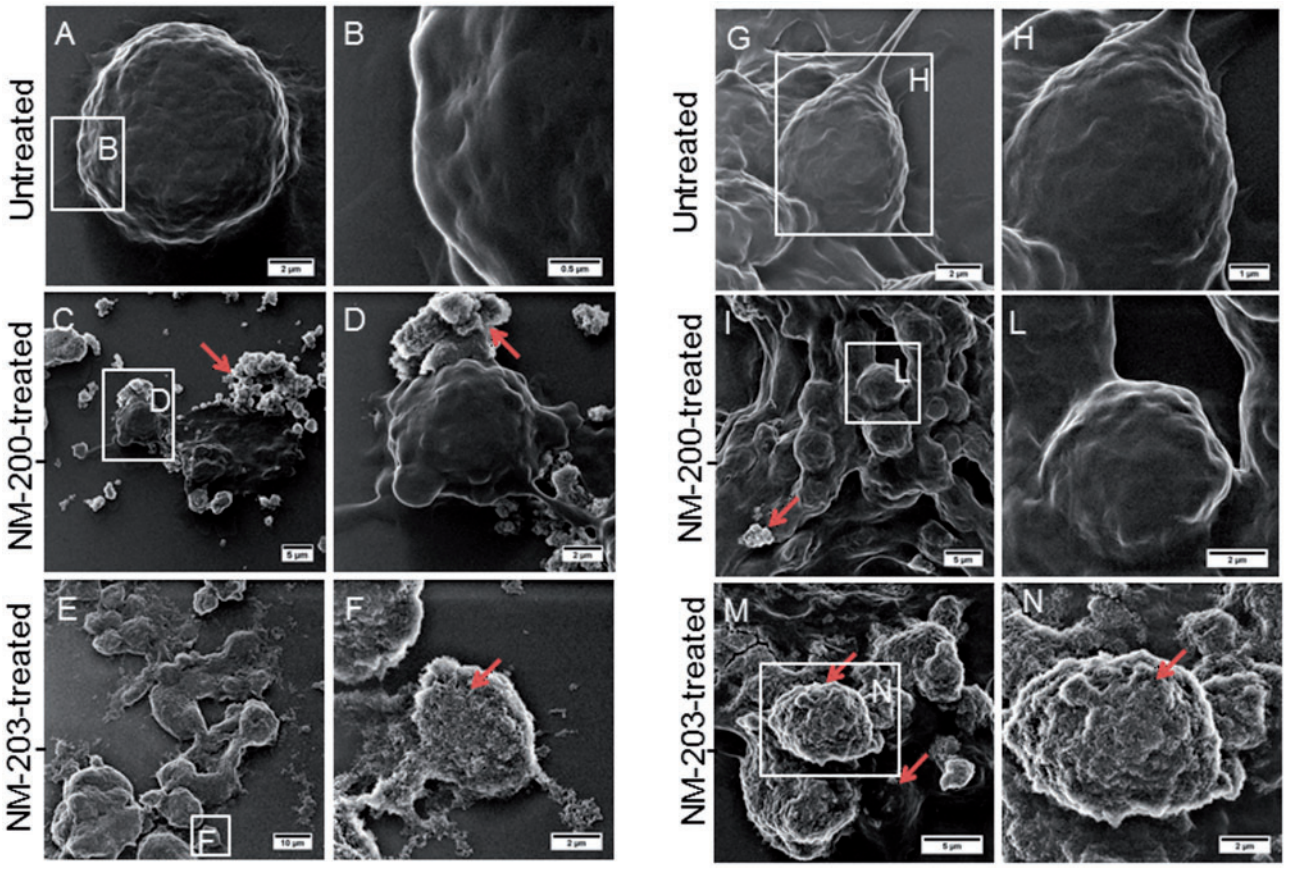

FIG. 2. He-ion microscopy (HIM) images of MH-S and RAW264.7. Cells, grown for 24 h in complete growth medium, were treated for 24 h with the indicated NM at 10 μg/cm^2 and imaged with He-ion microscopy (see Methods). A, B, Untreated MH-S; C, D, NM-200-treated MH-S; E, F, NM-203-treated MH-S cells; G, H) untreated RAW264.7; I–L) NM-200-treated RAW264.7; and M, N, NM-203-treated RAW264.7. C–F–I–N, Large ASNP agglomerates were visible, as well as partial or complete coverage of cell surface (as indicated by arrows). Images (B), (D), (F), (H), (L), and (N) are magnifications of images (A), (C), (E), (G), (I), and (M), respectively. Abbreviations: ASNP, amorphous silica nanoparticles; NM, nanomaterials.

Oxidative Stress in ASNP-Exposed Murine Macrophages

ROS production was measured on MH-S and RAW264.7 macrophage lines upon 24 h of incubation with NM-200 and NM-203 (Fig. 6). A significant dose-dependent increase of ROS production was detectable, by fluorescence signal recording, in NM-203-treated MH-S cells (Fig. 6A) but not in NM-203-treated RAW264.7 cells (Fig. 6B). Conversely, NM-200, did not promote ROS production either in MH-S cells or in RAW264.7 cells. The increase in fluorescence in MH-S cells treated with NM-203 was also evident by fluorescence microscopy (Fig. 6C and D).

Hmox-1 (hemeoxygenase-1) is known to play a major role in the cell response to oxidative stress-mediated injuries (Bhaskaran *et al.*, 2012). *Hmox1* expression was assessed after a 6 h-incubation with NM-200 and NM-203. For both macrophage lines, a dose-dependent increase in expression of *Hmox1* messenger was evident for NM-203-treated cells, although in MH-S the increase of the messenger was much higher than in RAW264.7 cells (10- and 12-fold for 5 and 10 μg/cm^2 respectively for MH-S, and 6- and 9-fold induction for 5 and 10 μg/cm^2, respectively, for RAW264.7) (Fig. 6E and F). In contrast, for both MH-S and RAW264.7 cells, NM-200 induced an increase in expression of the *Hmox1* messenger only at a concentration of 10 μg/cm^2, with a much lower effect for RAW264.7 cells.

The expression of *Hmox1* and *Tnf* was assessed after 8 h in RAW264.7 cells exposed to 10 μg/cm^2 of ASNP in the absence or in the presence of the antioxidant N-acetyl-cysteine (NAC, 1 mM). NAC significantly blunted the induction of *Tnf* in macrophages incubated with NM-203, but not with NM-200, although lowered *Hmox1* induction by both materials (from 4-fold to 2-fold for NM-200 and from 11-fold to 5-fold for NM-203, Fig. 6G and H).

DISCUSSION

The results presented in this study indicate that pyrogenic NM-203 ASNP are more biologically reactive than precipitated NM-200 ASNP. In particular, NM-203 resulted more cytotoxic and exhibit larger effects on macrophage activation than NM-200, suggesting that the thermally produced synthetic amorphous silica is correlated to the presence of crucial determinants of biological responses.

The identification of structural determinants of nanomaterial toxicity is greatly aided by the comparison of biological effects of different preparations of the same nanoparticles. However, to derive clear cut conclusions, the comparison should be ideally performed between nanomaterials differing by a single property only. In the present study, this principle has been applied to the evaluation of the biological effects of precipitated and pyrogenic ASNP, differing only in the method of synthesis. The characterization of NM-200 and NM-203, obtained from the JRC Nanomaterials Repository, had indicated comparable values of specific surface area, size of primary particles and agglomerates, and zeta potential (Rasmussen *et al.*,

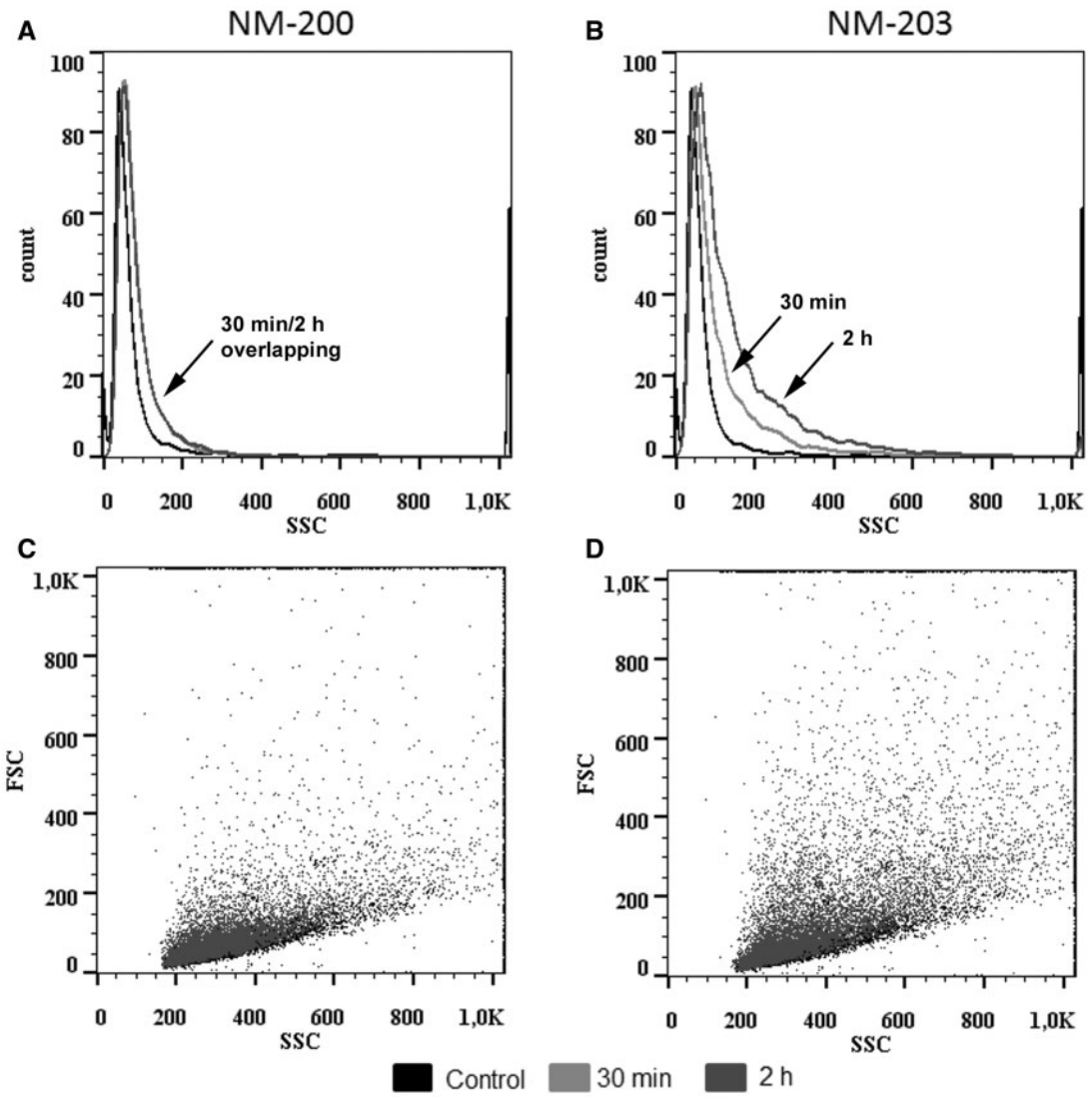

FIG. 3. Internalization of ASNP into RAW264.7 cells. Cells, grown for 24 h in complete growth medium, were treated with 5 μg/cm^2 of NM-200 (A–C) and NM-203 (B–D). After 30 min or 2 h of treatment, SSC was analyzed using FC500^{TM} flow cytometer (see Materials and Methods). Histograms of cells treated for 30 min or 2 h, as indicated. In A the lines of 30 min and 2 h are overlapping (A, B). Representative cytograms at 2 h (C, D). Black dots, control, untreated cells. Abbreviations: SSC, side scatter.

2013). We have integrated those data, showing that in FBS-supplemented media, ie, under the conditions adopted for biological experiments, NTA measurements did not show significant differences in the hydrodynamic radius between NM-200 and NM-203. Moreover, no significant further agglomeration was detected in this complex dispersing medium over a 24 h incubation. These data suggest that differences detected in the biological responses following cell incubation with NM-200 and NM-203 are not attributable to the different agglomeration of the 2 materials.

The different production processes lead to different surface chemistries with oxidative reactivity for NM-203 and null or reductive reactivity for NM-200 (Rasmussen *et al.*, 2013). In a protein-rich medium, different surface reactivity could modify the formation of protein corona, which is known to be a powerful determinant of the biological interactions of the nanomaterials (Ge *et al.*, 2015). The adsorption of proteins to ASNP has been previously investigated (Turci *et al.*, 2010) but no comparison was made in that study between pyrogenic and precipitated silica. The direct comparison between the 2 ASNP performed here (Fig. 1) not only indicated that pyrogenic ASNP bound a larger quantity of serum proteins than precipitated silica but also showed that the pattern of adsorbed proteins was not the same in the 2 cases. As Turci *et al.* (2010) reported, the adsorption of a protein on a surface is a very complex process that results from a contribution of energetic (hydrogen bonding, electrostatic forces, and hydrophobic interactions) and entropic factors (structural changes in the protein and dehydration of the protein and surface). In our case, the zeta potential values of the 2 ASNP were very similar; therefore we can exclude surface charge as the main reason of different uptake and specificity towards single serum protein. Zhang *et al.* (2012) have argued that, although a wide range of ASNP are endowed with similar coverages of surface silanols, this does not exclude distinct toxicity profiles. The same authors demonstrate that a major determinant of the different toxicity of ASNP produced by thermal or wet routes derives from differences in the siloxane framework architecture, attributable to the synthesis conditions. In that study, the Stober wet method was used for the production of colloidal ASNP. If the hypothesis proposed by Zhang *et al.* would

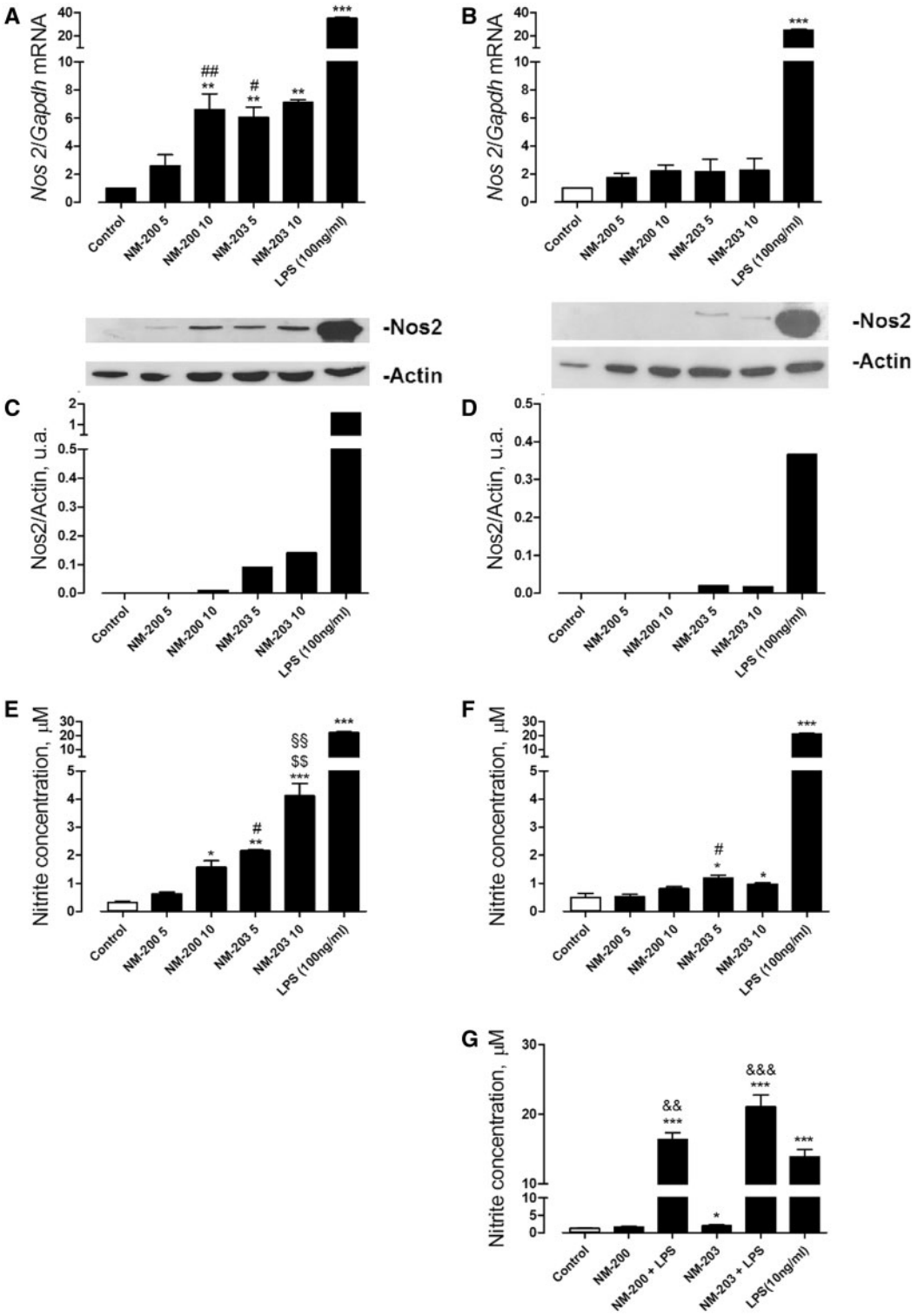

FIG. 4. Effects of NM-200 and NM-203 on *Nos2* expression and NO production in MH-S and RAW264.7 cells. For (A), (B), (C), (D), (E), and (F), cells, MH-S and RAW264.7 cells, grown for 24h in complete growth medium, were treated with 5 or 10 µg/cm^2 of NM-200 and NM-203, or with LPS (100 ng/ml), used as a positive control. A, B, After 24 h of treatment, mRNA was extracted and the expression of *Nos2* evaluated as described in Materials and Methods. C, D, The expression of the protein Nos2 was assessed through Western Blot in cultures treated in parallel and extracted after 48 h of treatment. A representative blot is shown, with actin used for loading control (upper panel). In the lower panel the densitometric analysis of the same blot is shown. The experiment was performed twice with comparable results. E, F, Nitrite concentration was determined in the culture medium of the cells used for the experiment shown in (C, D). For (G), RAW264.7 were treated with 10 µg/cm^2 of NM-200 or NM-203 in the absence or in the presence of LPS (10 ng/ml). After 48 h of treatment, nitrite concentration was determined in the culture medium. For (A) and (B), data are means ± SD of 2 independent determinations, each performed twice. For (E) and (F), data are means of 4 independent determinations ± SD. For (G), data are means ± SD of 3 independent determinations. *$P < .05$, **$P < .01$ and ***$P < .001$ versus untreated, control cells. #$P < .05$ and ##$P < .01$ versus 5 µg/cm^2 of NM-200. $$$P < .01$ versus 10 µg/cm^2 of NM-200. §§$P < .01$ versus 5 µg/cm^2 of NM-203. £££$P < .01$ and £££$P < .001$ versus LPS. Abbreviations: ASNP, amorphous silica nanoparticles; A.U., arbitrary units; *Gapdh*, Glyceraldehyde 3-phosphate dehydrogenase (gene); LPS, lipopolysaccharide; NM, nanomaterials; Nos2, inducible nitric oxide synthetase; SD, standard deviation.

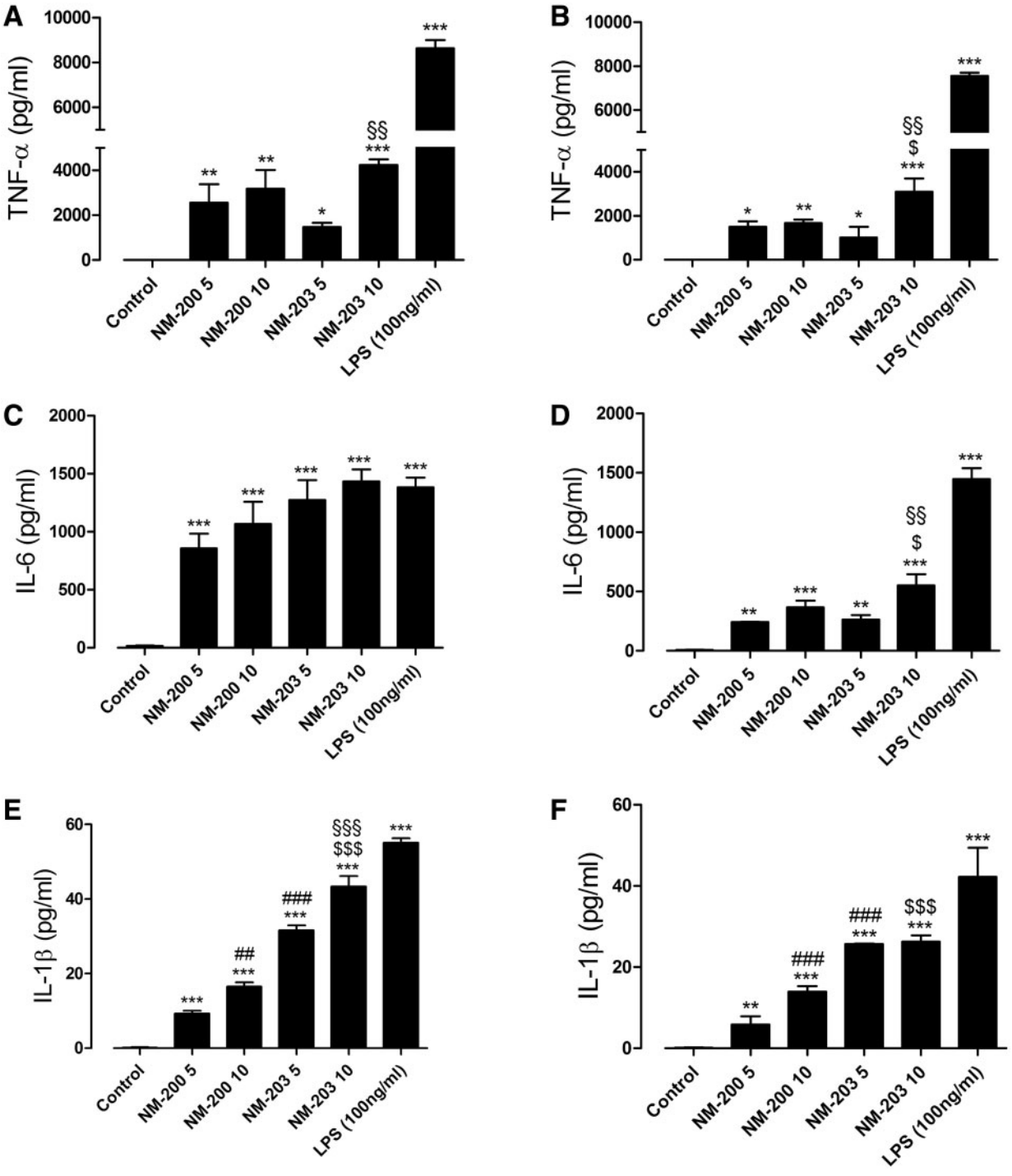

FIG. 5. TNF-α, IL-6, and IL-1β secretion in MH-S and RAW264.7 cells. Cells, grown for 24 h in complete growth medium, were treated with 5 or 10 μg/cm^2 of NM-200 or NM-203 or with LPS (100 ng/ml), as a positive control. After 6, 12, or 48 h of treatment, for TNF-α, IL-6, or IL-1β, respectively, the indicated cytokines were measured in the extracellular medium, as described under Materials and Methods. A, C, and E: MH-S; B, D, and F: RAW264.7. Data are means of 3 independent determinations ± SD. $^{**}P < .01$ and $^{***}P < .001$ versus untreated, control cells; $\#\#P < .01$ and $\#\#\#P < .001$ versus 5 μg/cm^2 of NM-200. $\$P < .05$, $\$\$P < .01$, and $\$\$\$P < .001$ versus 10 μg/cm^2 of NM-200. $\S\S P < .01$ and $\S\S\S P < .001$ versus 5 μg/cm^2 of NM-203. Abbreviations: IL-1β, interleukin-1beta; IL-6, interleukin-6; LPS, lipopolysaccharide; NM, nanomaterials; SD, standard deviation; TNF-α, tumor necrosis factor alpha.

be applicable also for the pyrogenic and precipitated ASNP tested in the present study, we could speculate that specific domains of serum proteins may have a structure that better fits the surface characteristics (ie, the siloxane framework) of the 2 ASNP preparations.

Nanoparticle surface may also adsorb organic molecules other than proteins, which may affect the biological interactions of the nanomaterials. For instance, we recently demonstrated that the interaction between TiO_2 NP and LPS strongly potentiates macrophage activation, suggesting that the

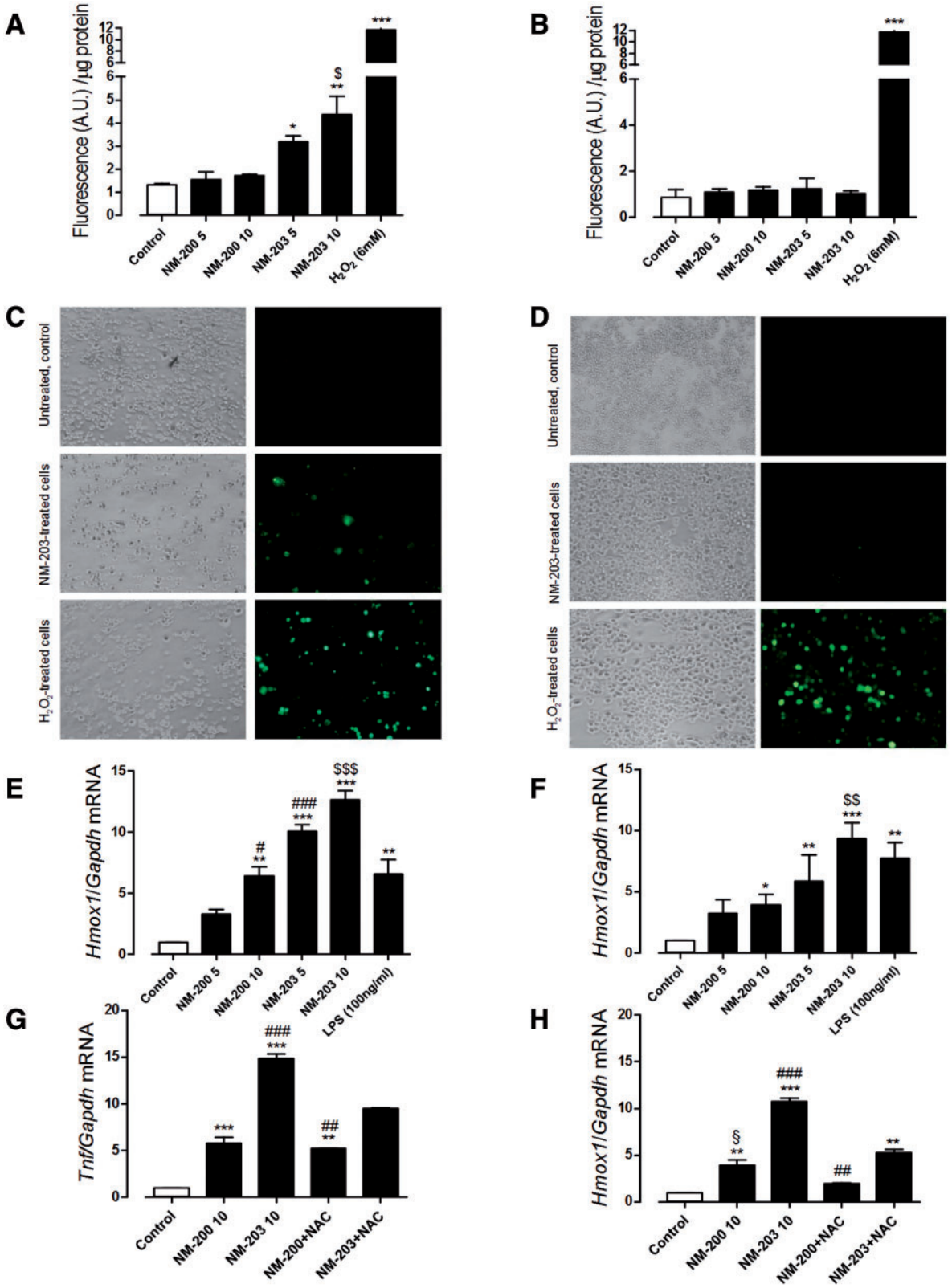

FIG. 6. ROS production, *Hmox1* and *Tnf* induction in macrophages. For (A), (B), (C), (D), cells, grown in complete growth medium, were treated with 5 or 10 µg/cm^2 of NM-200 or NM-203 or with H_2O_2 (6 mM), as a positive control (A) and (B). After 24 h of treatment, MH-S (A) or RAW264.7 cells (B) were incubated for 2 h with CM-H_2DCF-DA (5 µM). Fluorescence was determined as described under Materials and Methods. Data are means ± SD of 3 independent determinations, each performed twice, $^*P < .05$, $^{**}P < .01$ and $^{***}P < .001$ versus untreated, control cells; $\$P < .05$ versus 10 µg/cm^2 of NM-200. (C, D) Before the determination of cell CM-H_2DCF-DA, images of representative fields were taken in phase contrast or with fluorescence microscope. (C), MH-S; (D), RAW264.7 cells. × 100. (E, F) After 6 h of treatment with ASNP or LPS (100 ng/ml, positive control), mRNA was extracted and the expression of *Hmox1* evaluated as described in Materials and Methods. (E), MH-S; (F), RAW264.7. Data are means ± SD of 2 independent determinations, each performed twice. $^*P < .05$, $^{**}P < .01$, and $^{***}P < .001$ versus untreated, control cells; $\#P < .05$ and $\#\#\#P < .001$ versus 5 µg/cm^2 of

presence of environmental contaminants may enhance the proinflammatory activity of nanomaterials (Bianchi *et al.*, 2015). As far as ASNP are concerned, Shi *et al.* (2010) reported that LPS and ASNP have synergistic cytotoxic and oxidative effects on A549 lung epithelial cells. Our results demonstrate that ASNP enhanced LPS effects also on macrophage activation, with a much higher effect observed for the pyrogenic NM-203. Several mechanisms may underlie this synergy; the amount of LPS adsorbed may be larger for pyrogenic than for precipitated ASNP or LPS-induced activation may be indirectly favored by NM-203 effects on macrophages, for instance, through the promotion of a stronger oxidative stress.

The different surface reactivity stemming from different production processes may also influence the different interaction of the 2 ASNP with the cell surface. Indeed, Pavan *et al.* (2013) reported that the different interaction between various types of amorphous silica (pyrogenic, precipitated, vitreous) and red blood cells (RBC) is mainly determined by the surface arrangement of silanols and siloxanes that are able to match with epitopes present in the RBC membrane. The resulting hemolysis, evident for pyrogenic and vitreous but not for precipitated silica, could be correlated with the pathogenic responses to ASNP (Pavan *et al.*, 2013) and, at least for vitreous silica, with inflammasome activation (Pavan *et al.*, 2014). In our study, helium ion microscopy (Fig. 2) has been used to investigate the interaction of ASNP with the cell membrane. NM-203, but not NM-200, clearly formed aggregated layers onto the plasma membrane of both macrophage lines, so that the cell surface was completely or partially covered by ASNP. Close interaction with cell membrane of pyrogenic silica and changes in membrane morphology were reported previously by electron microscopy (Zhang *et al.*, 2012). However, no obvious differences between pyrogenic and precipitated ASNP internalization were found in macrophages with the same technique (Gazzano *et al.*, 2012). In contrast with those results, our cytofluorimetric analysis indicates that, at least at a short time of incubation, NM-203 enter cells more efficiently than NM-200 ASNP (Fig. 3).

All the inflammatory parameters tested (*Nos2* induction at both protein and gene level, NO production, TNF-α, IL-6, and IL-1β secretion) were more evident in NM-203- than in NM-200-treated macrophages. Importantly, although the effects were overall more evident in MH-S cells than in RAW 264.7 cells, the ranking of biological effects was consistently NM-203 > NM-200 in the 2 macrophage cell lines. Our results are consistent with recent studies that have reported higher cytotoxicity and inflammatory activity of pyrogenic, as compared to precipitated or colloidal ASNP, towards macrophages (Gazzano *et al.*, 2012; Sandberg *et al.*, 2012; Zhang *et al.*, 2012). Although we do not specifically investigate the activation modality elicited by ASNP, all the parameters taken into consideration are consistent with M1 or "classical" macrophage activation, a coordinated response at transcriptional level that plays a major role in promoting acute inflammation. It is known that M1 activation of inflammatory cells is associated with oxidative stress (Park and Park, 2009). Thus, the higher cytotoxicity and the greater proinflammatory responses induced by NM-203 in both macrophage cell lines may be due to the higher oxidative stress withstood by cells exposed to this material. In support of our hypothesis, we have demonstrated that pyrogenic ASNP are more powerful inducers of *Hmox1* than precipitated ASNP. Given that *Hmox1* induction is one of the most sensitive and reliable indicators of the cell response to oxidative stress and a parameter linked to inflammation triggering (Naito *et al.*, 2014; Poss and Tonegawa 1997), these results indicate that NM-203-treated cells undergo a higher level of oxidative stress than NM-200-treated cells, a conclusion also supported by the results of the CM-H_2DCF fluorescence test (Fig. 6). The role of oxidative stress in the response to ASNP is also supported by the effects of the antioxidant NAC, which partially hinders, along with *Hmox1* expression, also *Tnf* induction in NM203-treated cells. However, this partial inhibition, along with the NAC insensitivity of the NM-200-dependent stimulation of *Tnf* induction, suggests that ASNP promote cytokine production through a complex mechanism only in part attributable to oxidative stress.

A significant dose-dependent increase in IL-1β secretion was detected in macrophages exposed to ASNP. Such response was particularly evident in NM-203-treated macrophages, and pointed to the activation of the inflammasome, as already reported in previous studies from other research groups. However, those studies were performed on THP-1 cells activated with phorbol esters (Zhang *et al.*, 2012) or on RAW264.7 cells primed by LPS (Sandberg *et al.*, 2012) and exposed to high doses of pyrogenic ASNP (50-200 μg/ml). Conversely, in our study we demonstrated the activation of inflammasome in non-primed macrophages exposed to relatively low, barely toxic doses of pyrogenic ASNP. Moreover, for the first time, our results also show the activation of this pathway by precipitated ASNP, although with a smaller potency compared with pyrogenic silica. Since maturation of IL-1β is tightly regulated by the NLRP3 inflammasome, our results suggest that even low doses of pyrogenic and precipitated nanoparticles are able to stimulate both *Il1* expression and proIL-1β processing.

In conclusion, the data presented in this study demonstrate that pyrogenic NM-203 are more cytotoxic and proinflammatory than precipitated NM-200 of comparable size and surface area. Taking into account also the literature data as outlined above, the greater biological reactivity of pyrogenic ASNP does not seem to depend on a different agglomeration behaviour when dispersed in biological media but may, instead, derive from their higher surface reactivity associated with a higher capability to: (1) adsorb proteins and, possibly, other bioactive organic molecules, (2) interact with cell membranes, and (3) induce oxidative stress in exposed cells. With this in mind, lowering the particle surface reactivity should be considered as part of the "safety by design" approaches to reduce biological hazard derived from exposure to pyrogenic ASNP. Moreover, as substantiated above, the biological reactivity of pyrogenic and precipitated ASNP should be presumed to be different and, in our opinion, there is thus a need for a labelling that would report the method of synthesis when ASNP are present in food and, possibly, in other products.

ACKNOWLEDGMENTS

The authors declare that they have no competing interests.

NM-200; $$P < .01 and $$$P < .001 versus 10 μg/cm^2 of NM-200. (G, H), RAW264.7 cells were treated for 8 h with 10 μg/cm^2 of NM-200 or NM-203. As indicated, NAC (1 mM) was added 1 h before the incubation with ASNP and maintained throughout the experiment. At the end of the incubation, mRNA was extracted, and the expression of *Tnf* (G) and *Hmox1* (H) was evaluated as described in Materials and Methods. Data are means ± SD of 3 independent determinations. **P < .01 and ***P < .001 versus untreated, control cells; ##P < .01 and ###P < .001 versus NM-203 + NAC; §P < .05 versus NM-200 + NAC. Abbreviations: ASNP, amorphous silica nanoparticles; A.U., arbitrary units; CM-H_2DCF-DA,5 -(and-6)-chloromethyl-2′,7′ dichlorodihydrofluorescein diacetate, acetyl ester; *Hmox1*, Hemeoxygenase 1 (gene); H_2O_2, oxygen peroxyde; LPS, lipopolysaccharide; NAC, N-acetyl-cysteine; NM, nanomaterials; SD, standard deviation; *Tnf*, tumor necrosis factor-alpha (gene).

SUPPLEMENTARY DATA

Supplementary data are available online at http://toxsci.oxfordjournals.org/.

FUNDING

NANoREG (FP7-NMP2012 310584); MaRiNa (FP7-NMP4-LA-2011-26321); QNANO TCD-TA136 (INFRA-2010-1.1.31-262163).

REFERENCES

Alinovi, R., Goldoni, M., Pinelli, S., Campanini, M., Aliatis, I., Bersani, D., Lottici, P. P., Iavicoli, S., Petyx, M., Mozzoni, P., *et al*. (2015). Oxidative and pro-inflammatory effects of cobalt and titanium oxide nanoparticles on aortic and venous endothelial cells. *Toxicol. In Vitro* **29**, 426–437.

Arts, J. H., Muijser, H., Duistermaat, E., Junker, K., and Kuper, C. F. (2007). Five-day inhalation toxicity study of three types of synthetic amorphous silicas in Wistar rats and post-exposure evaluations for up to 3 months. *Food Chem. Toxicol.* **45**, 1856–1867.

Athinarayanan, J., Periasamy, V. S., Alsaif, M. A., Al-Warthan, A. A., and Alshatwi, A. A. (2014). Presence of nanosilica (E551) in commercial food products: TNF-mediated oxidative stress and altered cell cycle progression in human lung fibroblast cells. *Cell Biol Toxicol.* **30**, 89–100.

Bhaskaran, N., Shukla, S., Kanwal, R., Srivastava, J. K., and Gupta, S. (2012). Induction of heme oxygenase-1 by chamomile protects murine macrophages against oxidative stress. *Life. Sci.* **90**, 1027–1033.

Bianchi, M. G., Allegri, M., Costa, A. L., Blosi, M., Gardini, D., Del Pivo, C., Prina-Mello, A., Cristo Di, Bussolati, L., and Bergamaschi, O.E. (2015). Titanium dioxide nanoparticles enhance macrophage activation by LPS through a TLR4-dependent intracellular pathway. *Toxicol. Res.* **4**, 385–398.

Birmingham, A., Selfors, L. M., Forster, T., Wrobel, D., Kennedy, C. J., Shanks, E., Santoyo-Lopez, J., Dunican, D. J., Long, A., Kelleher, D., *et al.* (2009). Statistical methods for analysis of high-throughput RNA interference screens. *Nat. Methods* **6**, 569–575.

Farcal, L., Torres Andon, F., Di Cristo, L., Rotoli, B. M., Bussolati, O., Bergamaschi, E., Mech, A., Hartmann, N. B., Rasmussen, K., Riego-Sintes, J., *et al*. (2015). Comprehensive in vitro toxicity testing of a panel of representative oxide nanomaterials: first steps towards an intelligent testing strategy. *PLoS One* **10**, e0127174.

Farinha, C. M., Mendes, F., Roxo-Rosa, M., Penque, D., and Amaral, M. D. (2004). A comparison of 14 antibodies for the biochemical detection of the cystic fibrosis transmembrane conductance regulator protein. *Mol. Cell Probes* **18**, 235–242.

Fubini, B., and Hubbard, A. (2003). Reactive oxygen species (ROS) and reactive nitrogen species (RNS) generation by silica in inflammation and fibrosis. *Free Radic. Biol. Med.* **34**, 1507–1516.

Gazzano, E., Ghiazza, M., Polimeni, M., Bolis, V., Fenoglio, I., Attanasio, A., Mazzucco, G., Fubini, B., and Ghigo, D. (2012). Physicochemical determinants in the cellular responses to nanostructured amorphous silicas. *Toxicol. Sci.* **128**, 158–170.

Ge, C., Tian, J., Zhao, Y., Chen, C., Zhou, R., and Chai, Z. (2015). Towards understanding of nanoparticle-protein corona. *Arch. Toxicol.* **89**, 519–539.

Guichard, Y., Fontana, C., Chavinier, E., Terzetti, F., Gate, L., Binet, S., and Darne, C. (2015). Cytotoxic and genotoxic evaluation of different synthetic amorphous silica nanomaterials in the V79 cell line. Toxicol. Ind. Health. In press. doi:10.1177/0748233715572562.

Hole, P., Sillence, K., Hannell, C., Maguire, C. M., Roesslein, M., Suarez, G., Capracotta, S., Magdolenova, Z., Horev-Azaria, L., Dybowska, A., *et al*. (2013). Interlaboratory comparison of size measurements on nanoparticles using nanoparticle tracking analysis (NTA). *J. Nanopart Res.* **15**, 2101.

Kaewamatawong, T., Kawamura, N., Okajima, M., Sawada, M., Morita, T., and Shimada, A. (2005). Acute pulmonary toxicity caused by exposure to colloidal silica: particle size dependent pathological changes in mice. *Toxicol. Pathol.* **33**, 743–749.

Kozak, K., Bakos, G., Hoff, A., Bennett, E., Dunican, D., Davies, A., Kelleher, D., Long, A., and Csucs, G. (2010). Workflow-based software environment for large-scale biological experiments. *J. Biomol. Screen.* **15**, 892–899.

Lin, W., Huang, Y. W., Zhou, X. D., and Ma, Y. (2006). In vitro toxicity of silica nanoparticles in human lung cancer cells. *Toxicol. Appl. Pharmacol.* **217**, 252–259.

Mohamed, B. M., Verma, N. K., Prina-Mello, A., Williams, Y., Davies, A. M., Bakos, G., Tormey, L., Edwards, C., Hanrahan, J., Salvati, A., *et al.* (2011). Activation of stress-related signalling pathway in human cells upon SiO2 nanoparticles exposure as an early indicator of cytotoxicity. *J. Nanobiotechnol.* **9**, 29.

Morishige, T., Yoshioka, Y., Inakura, H., Tanabe, A., Yao, X., Narimatsu, S., Monobe, Y., Imazawa, T., Tsunoda, S., Tsutsumi, Y., *et al.* (2010a). The effect of surface modification of amorphous silica particles on NLRP3 inflammasome mediated IL-1beta production, ROS production and endosomal rupture. *Biomaterials* **31**, 6833–6842.

Morishige, T., Yoshioka, Y., Inakura, H., Tanabe, A., Yao, X., Tsunoda, S., Tsutsumi, Y., Mukai, Y., Okada, N., and Nakagawa, S. (2010b). Cytotoxicity of amorphous silica particles against macrophage-like THP-1 cells depends on particle-size and surface properties. *Pharmazie* **65**, 596–599.

Movia, D., Prina-Mello, A., Bazou, D., Volkov, Y., and Giordani, S. (2011). Screening the cytotoxicity of single-walled carbon nanotubes using novel 3D tissue-mimetic models. *ACS Nano* **5**, 9278–9290.

Movia, D., Prina-Mello, A., Volkov, Y., and Giordani, S. (2010). Determination of spiropyran cytotoxicity by high content screening and analysis for safe application in bionanosensing. *Chem. Res. Toxicol.* **23**, 1459–1466.

Naito, Y., Takagi, T., and Higashimura, Y. (2014). Heme oxygenase-1 and anti-inflammatory M2 macrophages. *Arch. Biochem. Biophys.* **564**, 83–88.

Napierska, D., Thomassen, L. C., Lison, D., Martens, J. A., and Hoet, P. H. (2010). The nanosilica hazard: another variable entity. *Part Fibre Toxicol.* **7**, 39.

Nishimori, H., Kondoh, M., Isoda, K., Tsunoda, S., Tsutsumi, Y., and Yagi, K. (2009). Silica nanoparticles as hepatotoxicants. *Eur. J. Pharm. Biopharm.* **72**, 496–501.

Park, E. J., and Park, K. (2009). Oxidative stress and pro-inflammatory responses induced by silica nanoparticles in vivo and in vitro. *Toxicol. Lett.* **184**, 18–25.

Pavan, C., Rabolli, V., Tomatis, M., Fubini, B., and Lison, D. (2014). Why does the hemolytic activity of silica predict its pro-inflammatory activity? *Part Fibre Toxicol.* **11**, 76.

Pavan, C., Tomatis, M., Ghiazza, M., Rabolli, V., Bolis, V., Lison, D., and Fubini, B. (2013). In search of the chemical basis of the hemolytic potential of silicas. *Chem. Res. Toxicol.* **26**, 1188–1198.

Poss, K. D., and Tonegawa, S. (1997). Reduced stress defense in heme oxygenase 1-deficient cells. *Proc. Natl. Acad. Sci. USA* **94**, 10925–10930.

Prina-Mello, A., Crosbie-Staunton, K., Salas, G., Morales, M. D., and Volkov, Y. (2013). Multiparametric toxicity evaluation of SPIONs by high content screening technique: identification of biocompatible multifunctional nanoparticles for nanomedicine. *IEEE Trans. Magnetics* **49**, 377–382.

Prina-Mello, A., Mohamed, B. M., Verma, N. K., Jain, N., and Volkov, Y. (2014). Advanced methodologies and techniques for assessing nanomaterial toxicity: from manufacturing to nanomedicine screening. In *Nanotoxicology: Progress Toward Nanomedicine*. (N. A. Monteiro-Riviere and L. C. Tran Eds.), 2nd ed., pp. 155–176. CRC Press, Boca Raton, FL.

Rasmussen, K., Mech, A., Mast, J., De Temmerman, P.-J., Waegeneers, N., VanSteen, F., Pizzolon, J. C., De Temmerman, L., Van Doren, E., Jensen, K. A., *et al.* (2013). Synthetic Amorphous Silicon Dioxide (NM-200, NM-201, NM-202, NM-203, NM-204): Characterisation and Physico-Chemical Properties. JRC Repository: NM-series of Representative Manufactured Nanomaterials. JRC Scientific Policy Reports.

Sala, R., Rotoli, B. M., Colla, E., Visigalli, R., Parolari, A., Bussolati, O., Gazzola, G. C., and Dall'Asta, V. (2002). Two-way arginine transport in human endothelial cells: TNF-alpha stimulation is restricted to system y(+). *Am. J. Physiol. Cell Physiol.* **282**, C134–C143.

Sandberg, W. J., Lag, M., Holme, J. A., Friede, B., Gualtieri, M., Kruszewski, M., Schwarze, P. E., Skuland, T., and Refsnes, M. (2012). Comparison of non-crystalline silica nanoparticles in IL-1beta release from macrophages. *Part Fibre Toxicol.* **9**, 32.

Sayes, C. M., Reed, K. L., and Warheit, D. B. (2007). Assessing toxicity of fine and nanoparticles: comparing in vitro measurements to in vivo pulmonary toxicity profiles. *Toxicol. Sci.* **97**, 163–180.

Shi, Y., Yadav, S., Wang, F., and Wang, H. (2010). Endotoxin promotes adverse effects of amorphous silica nanoparticles on lung epithelial cells in vitro. *J. Toxicol. Environ. Health A* **73**, 748–756.

Tavares, A. M., Louro, H., Antunes, S., Quarre, S., Simar, S., De Temmerman, P. J., Verleysen, E., Mast, J., Jensen, K. A., Norppa, H., Nesslany, F., *et al.* (2014). Genotoxicity evaluation of nanosized titanium dioxide, synthetic amorphous silica and multi-walled carbon nanotubes in human lymphocytes. *Toxicol. In Vitro* **28**, 60–69.

Turci, F., Ghibaudi, E., Colonna, M., Boscolo, B., Fenoglio, I., and Fubini, B. (2010). An integrated approach to the study of the interaction between proteins and nanoparticles. *Langmuir* **26**, 8336–8346.

van der Zande, M., Vandebriel, R. J., Groot, M. J., Kramer, E., Herrera Rivera, Z. E., Rasmussen, K., Ossenkoppele, J. S., Tromp, P., Gremmer, E. R., Peters, R. J., *et al.* (2014). Sub-chronic toxicity study in rats orally exposed to nanostructured silica. *Part Fibre Toxicol.* **11**, 8.

Williams, Y., Byrne, S., Bashir, M., Davies, A., Whelan, A., Gun'ko, Y., Kelleher, D., and Volkov, Y. (2008). Comparison of three cell fixation methods for high content analysis assays utilizing quantum dots. *J. Microsc.* **232**, 91–98.

Zhang, H., Dunphy, D. R., Jiang, X., Meng, H., Sun, B., Tarn, D., Xue, M., Wang, X., Lin, S., Ji, Z., *et al.* (2012). Processing pathway dependence of amorphous silica nanoparticle toxicity: colloidal vs pyrolytic. *J. Am. Chem. Soc.* **134**, 15790–15804.

Zhao, X., and Ibuki, Y. (2015). Evaluating the toxicity of silver nanoparticles by detecting phosphorylation of histone H3 in combination with flow cytometry side-scattered light. *Environ. Sci. Technol.* **49**, 5003–5012.